The role of two types of trellis layer for metal–insulator transition and antiferromagnetic order in the one-dimensional conductor V_6O_{13}

2004 J. Phys.: Condens. Matter 16 7863

(http://iopscience.iop.org/0953-8984/16/43/025)

INSTITUTE OF PHYSICS PUBLISHING JOURNAL OF PHYSICS: CONDENSED MATTER

J. Phys.: Condens. Matter **16** (2004) 7863–7871 PII: S0953-8984(04)78481-7

The role of two types of trellis layer for metal–insulator transition and antiferromagnetic order in the one-dimensional conductor V_6O_{13}

Masashige Onoda[1], **Toshio Ohki**[1] **and Yoshishige Uchida**[2]

[1] Institute of Physics, University of Tsukuba, Tennodai, Tsukuba 305-8571, Japan
[2] Superconducting Materials Center, National Institute for Materials Science, Namiki, Tsukuba 305-0044, Japan

E-mail: onoda@sakura.cc.tsukuba.ac.jp

Received 26 March 2004
Published 15 October 2004
Online at stacks.iop.org/JPhysCM/16/7863
doi:10.1088/0953-8984/16/43/025

Abstract

V_6O_{13} with a metal–insulator transition at $T_c \simeq 150$ K and an antiferromagnetic order at $T_N \simeq 50$ K has a d_{yz}-type single trellis layer and a d_{xy}-type double trellis layer, where x and y correspond to the a- and b-axis, respectively. Magnetic properties above T_c are consistent with theoretical results for a one-dimensional Hubbard model with the uniform electron concentration and a bandwidth comparable to the effective on-site Coulomb energy. Below T_c, in the light of properties of δ-phase vanadium bronzes, the spin-singlet state is considered to appear in the double trellis layer and the one-dimensional Heisenberg chain-like state is formed in the single layer, accompanied with valence order; and at T_N, the antiferromagnetic order takes place in the single layer. The temperature dependence of the electrical resistivity for the one-dimensional chain above T_c is mainly due to antiferromagnetic spin fluctuations, and those for the normal directions nearly follow $1/T$ which is likely due to the renormalization effect of the Fermi surface by the fluctuations. The Hall coefficient above T_c is found to be roughly linear in T.

1. Introduction

Various transition-metal oxides with unfilled d-orbitals have been investigated to clarify properties of correlated electron systems and quantum spin-fluctuation systems. They are also utilized as various functional materials such as thermoelectric devices or rechargeable lithium batteries. These basic and applied properties are essentially related to the structures formed by the linkage of rigid units such as the TO_6 octahedra or TO_4 tetrahedra, where T is a transition metal atom.

V_6O_{13}, which is classified into the Wadsley phase of V_nO_{2n+1}, exhibits a first-order metal–insulator transition at $T_c \simeq 150$ K accompanied with significant decrease of magnetic

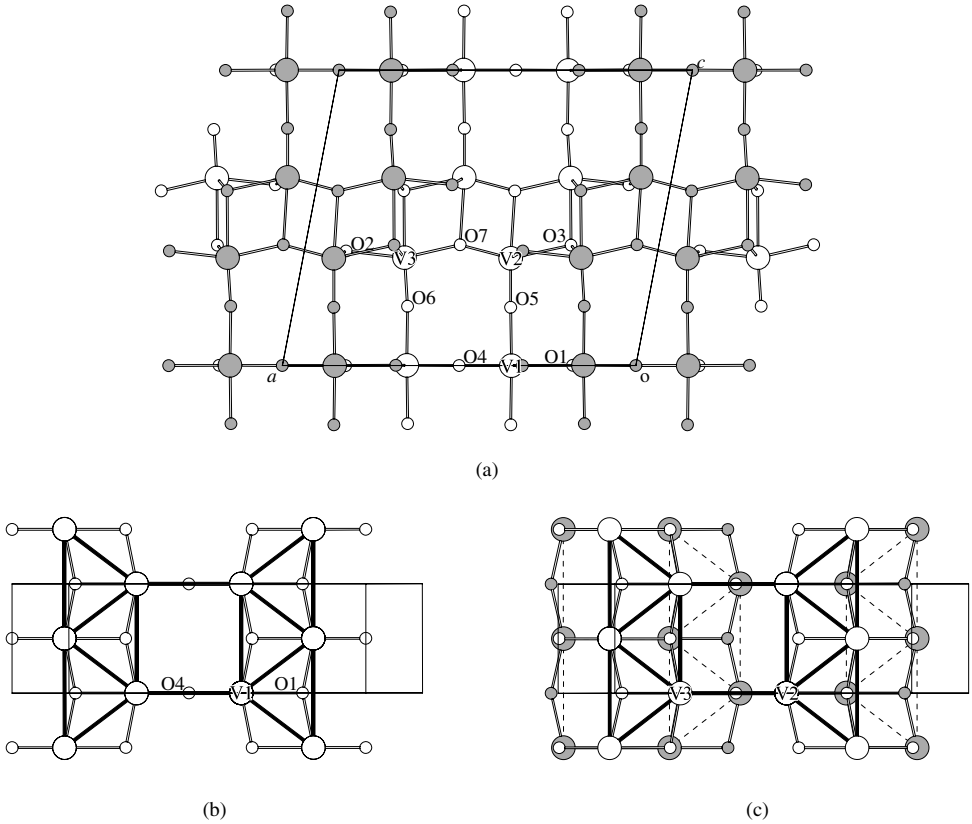

Figure 1. The crystal structure of V_6O_{13}: (a) the projection on the *ac*-plane; and (b, c) the projections on the *ab*-plane for the single layer and the double layer. Here, the open and shaded circles in (a) denote positions at $y = 0$ and $\frac{1}{2}$, respectively, and those in (c) are for $z \approx 0.4$ and 0.6. The thick and dotted lines in (b) and (c) indicate the V–V path at similar z levels.

susceptibility, and then undergoes an antiferromagnetic order at $T_N \simeq 50$ K [1–3]. This compound can also be utilized as cathode material in rechargeable lithium batteries [4]. Around eight lithium ions may be intercalated via an electrochemical reaction. Since the discharge–charge process of the batteries should correspond to the reduction–oxidation process of cathode materials, it will be possible to study detailed properties of the $Li_xV_6O_{13}$ system as a function of the concentration of d electrons from the basic science viewpoint.

The crystal structure with C2/m at room temperature above T_c is described with two types of layer of VO_6 octahedra parallel to the *ab*-plane as shown in figure 1; a single layer at $z = 0$ containing V1 (figure 1(b)) and a double layer at $z = \frac{1}{2}$ containing pairs of V2 and V3 (figure 1(c)) [5]. Here, the effective valencies of V1, V2 and V3 ions are approximately 4.16, 4.60 and 4.34, respectively [6]. The two layers are connected by corner-sharing oxygens. Although the single layer appears to be similar to the trellis layer in NaV_2O_5 [7], the ground-state wavefunctions are different from each other as will be discussed later. Below T_c, a mirror plane may be lost probably with a change of the valencies; 4.4, 4.4 and 4.2 for V1, V2 and V3, respectively, although details of the atomic parameters have not been revealed [6].

Electrical resistivity measurements indicated highly anisotropic behaviours with the lowest resistivity along the *b*-axis and suggested a quasi-one-dimensional electronic structure [1], which was recently confirmed by angle-resolved photoemission spectroscopy [7]. The

thermoelectric power measured for the *b*-axis was explained on the basis of the Hubbard narrow-band model with $W \ll U, W$ and U being bandwidth and the Coulomb repulsion energy, respectively [2]. NMR study for ^{51}V above T_c showed contributions from the spin fluctuations and the Korringa process [8]. In spite of these investigations, the role of two types of layer for the transitions at T_c and T_N remains unclear.

In this work, the site dependence of the effective valencies above T_c for V_6O_{13} is considered to be small; and thus the electrons are distributed uniformly at the concentration $N = \frac{2}{3}$, corresponding to the average valence 4.33. This approximation may be reasonable, since the effective valencies estimated with local oxygen coordinations are not significantly different from the average valency. A previous NMR study postulates that the V^{4+}-like signal above T_c is attributable to V1 and V3 sites, and the V^{5+}-like signal originated from V2 referring to crystallographic results [8]. However, the hyperfine field and the spin–lattice relaxation rate of the V^{5+}-like signal are too large for those of usual non-magnetic V^{5+} ions. Alternatively, the V^{4+}-like and V^{5+}-like signals assigned previously may be regarded as being those in the double trellis layer (V2 and V3) and the single layer (V1), respectively, taking account of local symmetry of oxygen coordinations.

This paper describes that magnetic properties above T_c can be explained using theoretical results for the one-dimensional Hubbard model with $W \simeq U$ and those below T_c are attributed to the formation of the spin-singlet state in the double layer as well as the one-dimensional Heisenberg chain-like state in the single layer accompanied by the valence order. Transport properties and the anisotropies above T_c are also explored in detail, where the anisotropy of the thermoelectric powers and the Hall coefficients are measured for the first time. Recently, the transport properties of one-dimensional conductors have attracted considerable attention, since due to a breakdown of the usual Fermi liquid theory caused by electron–electron interactions, the quasiparticle excitations are replaced by separate collective spin and charge excitations, each propagating with a different velocity [9].

2. Experiments

The polycrystalline specimens of V_6O_{13} were prepared by the solid-state reaction method. A mixture of $2V_2O_5$ (99.99%) and V_2O_3 that was made according to the procedure described in [10] were ground and pressed into pellets, which were sealed in quartz tubes, and then heated at 923 K for 48 h. The single-crystal specimens were grown through a chemical vapour transport with $TeCl_4$.

X-ray powder diffraction was performed through the θ–2θ scan method with Cu Kα radiation at temperatures between 80 and 300 K. X-ray four-circle diffraction with Mo Kα radiation was also done at 298 K. The four-terminal electrical resistivity between 80 and 450 K and the thermoelectric power between 80 and 300 K were measured by the DC method. In addition to the direct measurement for the anisotropy of the resistivity, the Montgomery technique [11] was applied. The Hall coefficient was obtained with magnetic fields from -7 to 7 T between 160 and 300 K. The magnetizations were measured using the Faraday method with a field of up to 1 T between 5 and 900 K, and the magnetic susceptibility was deduced from the linear part of the magnetization field curve with a decreasing field.

3. Results and discussion

3.1. Transport properties

Both the polycrystalline specimens and the single crystals with typical size $3(a) \times 7(b) \times 1(c^*)$ mm, $\boldsymbol{c}^*$ being defined as $\boldsymbol{a} \times \boldsymbol{b}$, are single phase. The cell dimensions with space group

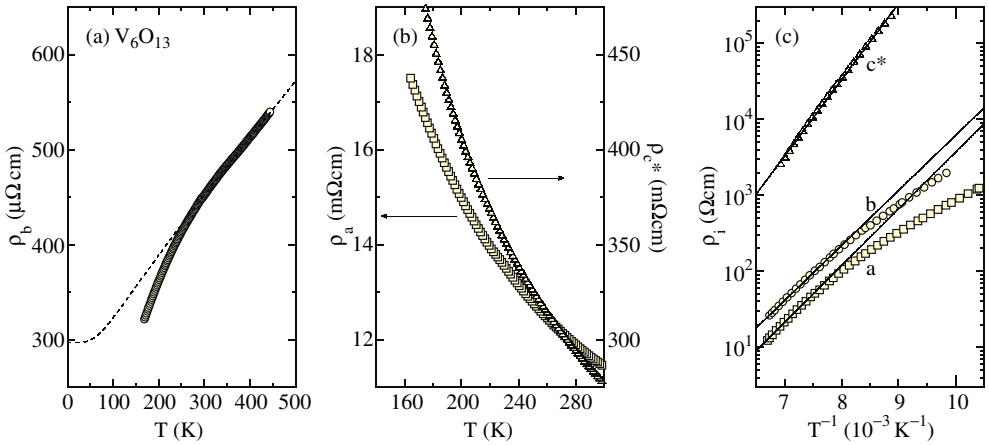

Figure 2. The temperature dependences of the electrical resistivities of V_6O_{13}: (a) *b*-axis for $T > T_c$ in the heated process; (b) *a*- and c^*-axis for $T > T_c$ in the cooled process; and (c) *a*-, *b*- and c^*-axis for $T < T_c$ in the cooled process. The dotted curve in (a) denotes results calculated based on the Bloch–Grüneisen formula and the full lines in (c) are those from the semiconductor model.

(This figure is in colour only in the electronic version.)

C2/m at room temperature are determined as follows: for the polycrystalline specimens, $a = 11.922(1), b = 3.6806(5), c = 10.1406(7)$ Å and $\beta = 100.885(7)$ deg, and for the single crystals, $a = 11.926(1), b = 3.681(1), c = 10.145(1)$ Å and $\beta = 100.89(1)$ deg, which agree well with the previous results [5]. A significant jump of the cell dimensions at T_c [6] was also confirmed. The present crystal has T_c of 164 K on heating and 152 K on cooling as will be described later.

The temperature dependences of the electrical resistivities for the *b*-axis (ρ_b) and the normal directions (ρ_a and ρ_{c^*}) with the usual four-terminal method above T_c are shown in figures 2(a) and (b), respectively. The Montgomery method also gave similar results. In addition to highly anisotropic behaviours reported previously [1], several important characteristics are revealed: the metallic temperature dependence of ρ_b above T_c significantly changes around room temperature, and ρ_a and ρ_{c^*} have incoherent temperature dependences roughly linear in $1/T$. For ρ_b at high temperatures, a fit with equation $\rho = \rho_0 + \rho_{BG}$, where the first and second terms on the right-hand side are the residual resistivity and the Bloch–Grüneisen formula, respectively, provides $\rho_0 = 300$ $\mu\Omega$ cm with the Debye temperature $\omega_D = 400$ K as shown by the dotted curve in figure 2(a). This fit is not reasonable owing to the significantly large value of ρ_0. The transport mechanism through strong antiferromagnetic spin fluctuations should be considered in order to explain the anomalous suppression of ρ_b at high temperatures [12]. The data for the *a*- and c^*-axis are likely explained with renormalization effects of the Fermi surface via antiferromagnetic spin fluctuations [12]. This mechanism has been postulated in order to account for the semiconductive temperature dependence of the resistivity normal to the CuO_2 plane in cuprate superconductors. Below T_c, semiconducting behaviours are observed for all of the directions as shown in figure 2(c); the energy gaps E_g for the *a*-, *b*- and c^*-axis estimated from the full lines with the equation $\rho \propto \exp(E_g/T)$ are 1722(10), 1668(8) and 2311(10) K, respectively. In this temperature region, the electron transport is two-dimensional with the highest resistivity along the c^*-axis.

The thermoelectric powers *S* for the *b*- and *a*-axis as a function of temperature are shown in figure 3. They are negative (electron-like) for $T > T_c$ and become nearly zero just at T_c

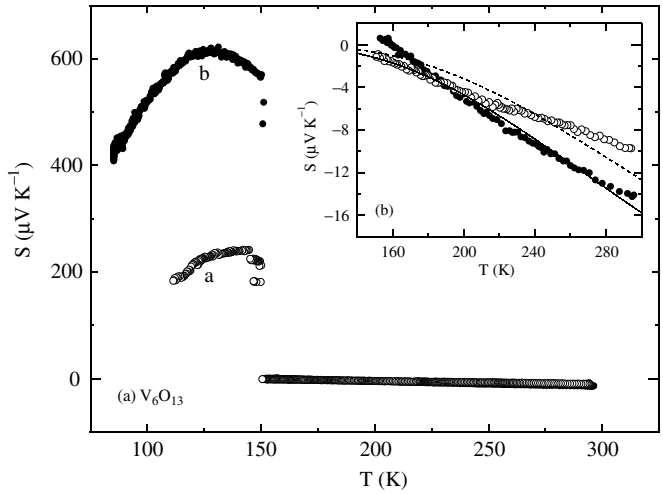

Figure 3. (a) The temperature dependences of the thermoelectric powers for the *b*- and *a*-axis of V_6O_{13} in the cooling process; (b) the detailed behaviours for $T > T_c$ with the curves calculated based on equation (1).

(figure 3(b)), while for $T < T_c$, they have large positive values (hole-like). Here, the data for the *b*-axis above T_c are similar to those published in [1, 2]. At first sight, it would be strange that the temperature dependences of S for the *b*- and *a*-axis at $T > T_c$ are roughly similar to each other. This is because the spin contributions are predominant and/or the electron transport for the *a*-axis in the present structure always involves the path for the *b*-axis, where ρ_b is significantly smaller than ρ_a.

The temperature dependences for $T > T_c$ are different than those expected from the Fermi-liquid theory. Following the analysis based on the Hubbard model with $W \ll U$ [2, 13], S is given by

$$S = \frac{k_B}{|e|}\left[\ln x - \frac{Ux^2}{T(e^{U/T} + x^2)}\right], \tag{1}$$

where

$$x = \frac{-1 + \sqrt{1 + 8e^{-U/T}}}{4e^{-U/T}},$$

for the uniform electron concentration $N = \frac{2}{3}$, k_B the Boltzmann constant and e the electron charge. The full curve for the *b*-axis and the dashed curve for the *a*-axis in figure 3(b) with this equation provide $U = 958(2)$ and $1052(4)$ K, respectively. These U values are a little larger than that for the *b*-axis estimated previously [2], and they are reasonable for d-type metals [14].

The origin of large positive values below T_c will be discussed in the next section, taking account of electronic states revealed through an analysis of magnetic properties. Considering the spin–charge separation in one-dimensional conductors, there exist two contributions of both the charge and spin excitations to the thermoelectric power. Detailed theoretical calculations for the temperature and electron-density dependences in the one-dimensional Hubbard model are desired.

Figure 4 indicates the Hall coefficients R for the *b*- and *a*-axis as a function of temperature. They are roughly linear in temperature as indicated by the dotted line, and have positive signs

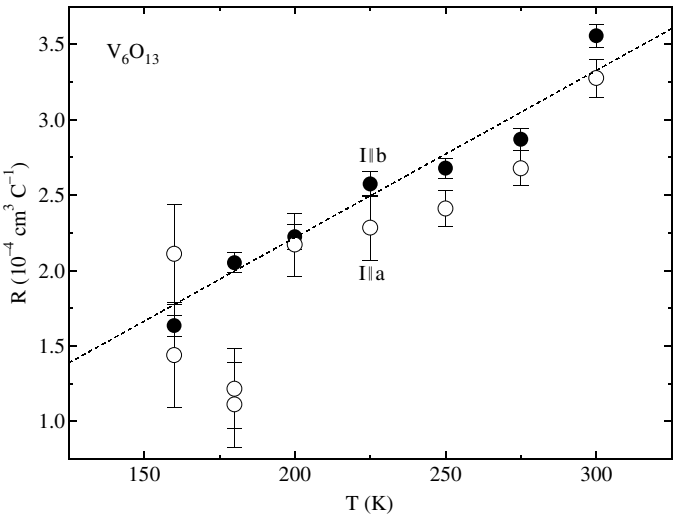

Figure 4. The temperature dependences of the Hall coefficients for the *b*- (full circles) and *a*-axis (open circles) of V_6O_{13} in the cooled process, where a fit for the former data with the dotted line gives $R = 1.1 \times 10^{-6}\,T\ \mathrm{cm}^3\ \mathrm{C}^{-1}$.

(hole-like) for $T > T_c$. The direction dependence of R is little. A band model with a constant scattering time over the Fermi surface [15] provides $|R| = 2.1 \times 10^{-4}$ cm^3 C^{-1}, which is quite close to the value at 180 K. However, the significant temperature dependence of R and the difference between signs of R and S suggest that the simple band model is not valid. Here, it should be noted that the power-law dependence of R has also been observed in the quasi one-dimensional organic conductor $(TMTSF)_2PF_6$ [16]. For this mechanism, a model where the electronic relaxation time varies over the Fermi surface has been postulated [17]. Anyway, in order to clarify the problem on the Hall effect relative to other transport properties revealed in this work, further investigations are necessary.

3.2. Magnetic properties

Figure 5 indicates the magnetic susceptibility χ as a function of temperature. Here, T_c and T_N defined as the temperatures at which the temperature-derivative for χ has a peak are: $T_c = 164(152)$ K on heating (cooling) and $T_N = 44$ K. A Curie–Weiss-like behaviour above T_c is considered on the basis of the one-dimensional Hubbard model. The results of the numerical calculation for the spin susceptibility χ_H with an arbitrary electron concentration in this model were presented in [18]. A fit shown by the full curve in figure 5(a) with the equation $\chi = \chi_H + \chi_0$, where χ_0 corresponds to the temperature-independent term from the Van Vleck and the diamagnetic components, provides the following parameters: $g = 1.914(5), t \equiv W/4 = 337(1)$ K and $\chi_0 = 7.9(1) \times 10^{-5}$ emu (mol V)$^{-1}$ for $N \simeq 0.7$ and $U/W = 1$. This g-factor nearly corresponds to the value for V^{4+} with a similar oxygen coordination [19, 20]. The increase of U/W leads to the decrease of g-factor. Thus, the metallic state of V_6O_{13} is found to have a bandwidth comparable with the effective Coulomb energy. The U value estimated above agrees roughly with that obtained from the thermoelectric power.

At around T_c, χ changes from 8.2 to 5.2×10^{-4} emu (mol V)$^{-1}$, which is attributed to the partial formation of the spin-singlet state. Let us assign which V site is responsible for this

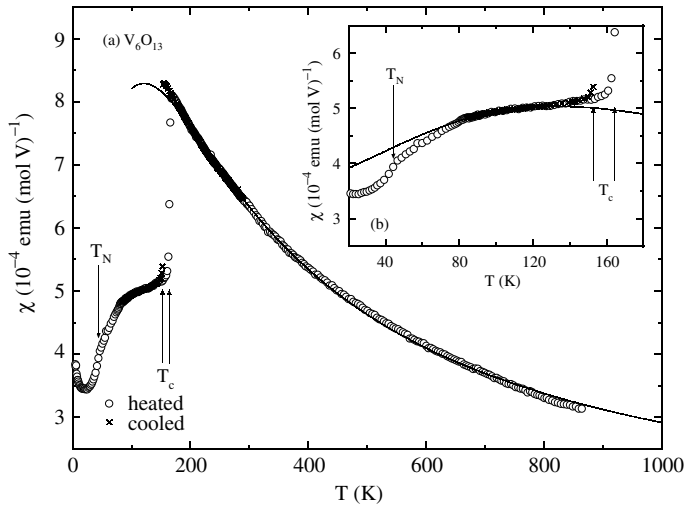

Figure 5. The temperature dependence of the magnetic susceptibility of V_6O_{13} in the heated and cooled processes: (a) all of the data and (b) the data for $T_N \sim T_c$. The full curves in (a) and (b) indicate results calculated on the basis of the one-dimensional Hubbard model and the one-dimensional Heisenberg model, respectively.

spin-gapped state. Using the Hartree–Fock function for V^{4+} [21], the ground-state wavefunctions for the V1, V2 and V3 sites above T_c are calculated to be $0.999d_{yz} - 0.008d_{xy}$, $-0.999d_{xy} - 0.027d_{yz}$ and $-0.962d_{xy} + 0.271d_{yz}$, respectively, where $\boldsymbol{x}\|\boldsymbol{a}$ and $\boldsymbol{y}\|\boldsymbol{b}$. For the single layer containing V1, the superexchange coupling through the oxygen p orbitals is effective only for the *b*-axis, which is clearly different from the case of MV_2O_5 [22], where the ground-state wavefunction is commonly d_{xy}-type, leading to three kinds of exchange couplings. On the other hand, for the double layer, both V2 and V3 have d_{xy}-type wavefunction, so that the superexchange couplings at a similar *z*-level in the *ab*-plane are expected to be most effective. Thus, the double trellis-layer model is applicable to this system, as shown in figure 1(c), where the thick lines and the dotted lines denote the V–V paths at similar and dissimilar *z*-levels, respectively. This network gives the spin-singlet ground state for an appropriate ratio of two kinds of corner-shared exchange coupling and the edge-shared coupling, as clarified for several δ-phase vanadium bronzes $M_xV_2O_5$ such as nearly $\frac{1}{6}$-filled $Ag_xV_2O_5$ with $x \simeq \frac{2}{3}$ [19] and nearly $\frac{1}{8}$-filled $Tl_xV_2O_5$ with $x \simeq \frac{1}{2}$ [20]. Although the structural transition takes place at around T_c, the spin network considered above may be still valid.

For the d_{yz}-type trellis layer, the antiferromagnetic exchange coupling is expected only for the *b*-axis. In effect, a round maximum behaviour reminiscent of low-dimensional spin systems seems to appear between T_c and T_N. Thus, neglecting the small spin contribution from the double trellis layer, χ is described in the form $\chi = \chi_{1D} + \chi_0$, where χ_{1D} denotes the one-dimensional Heisenberg spin susceptibility [23] originating from the d_{yz}-type trellis layer[3]. The full curve with this equation in figure 5(b) is drawn for the Curie constant $C_{1D} = 0.148(1)$ emu K (mol V)$^{-1}$ and the exchange coupling $J_{1D} = 205(1)$ K, where χ_0 is assumed to be the same with the value estimated above T_c. It should be noted that this C_{1D} roughly corresponds to the half-filled value for the single layer; 0.125 emu K (mol V)$^{-1}$ with $g = 2$. Therefore, it is expected that below T_c, the effective valencies of V1, V2 and V3 are

[3] The Heisenberg Hamiltonian is defined as $H = \sum_{\langle i,j \rangle} J\boldsymbol{S}_i \cdot \boldsymbol{S}_j$, with $\boldsymbol{S}_i$ being the spin operator at site *i*.

nearly 4, 4.5 and 4.5, respectively. The spin-singlet state for the double trellis layer may be regarded as being the ground state for a $\frac{1}{4}$-filled system.

4. Conclusions

Detailed transport measurements for V_6O_{13} with a metal–insulator transition at $T_c \simeq 150$ K and a Néel order at $T_N \simeq 50$ K indicate that the resistivity for the *b*-axis above T_c has a temperature dependence expected from the strong antiferromagnetic spin fluctuations, while those for the normal directions nearly follow $1/T$. The *negative* thermoelectric powers for the *b*- and *a*-axis above T_c are considered in terms of the Hubbard model in the atomic limit. The *positive* Hall coefficients for the *b*- and *a*-axis above T_c are found to be similar and roughly linear in T, comparable to the case of $(TMTSF)_2PF_6$. In order to establish a unified model for these transport properties in V_6O_{13}, further investigations are needed. In other words, the transport data revealed in this work are a touchstone of challenging theories for the one-dimensional electronic systems.

Magnetic properties above T_c are consistent with theoretical results for the one-dimensional Hubbard model with the uniform electron concentration and $U = W \simeq 1300$ K. This U value agrees roughly with that estimated on the basis of the thermoelectric power. Here, in order to obtain precise values of U and W from the thermoelectric power in the framework of the one-dimensional Hubbard model, detailed theoretical calculations with the spin–charge separation are necessary as pointed out above. Below T_c, with reference to the spin-gapped properties for the non-stoichiometric bronzes δ-$M_xV_2O_5$, the spin-singlet state is considered to appear in the d_{xy}-type double trellis layer and the one-dimensional Heisenberg chain-like state is formed in the d_{yz}-type single layer, accompanied with valence order. Here, the filling factor at the V1 site increases from $\frac{1}{3}$ to nearly $\frac{1}{2}$, while those of the V2 and V3 sites decrease to nearly $\frac{1}{4}$. The antiferromagnetic order at T_N may be originating from a weak interaction between the one-dimensional chains in the single layer [24]. In order to understand the experimental evidence that the $(1/2n)$-filled d_{xy}-type trellis layer with integer n often has spin-gapped properties, it may be important to consider the intersite correlation energy as well as a polaronic nature of electrons inherent to 3d transition-metal oxides, in addition to an on-site correlation energy.

A large jump of the thermoelectric power at T_c is of course due to the insulating nature of the system. The valence order described above may also contribute to this anomaly, since a slight deviation from a half-filled condition [13] or a half-filled condition [25] provides large *positive* thermoelectric powers.

Acknowledgment

We thank Dr Y Ohashi for stimulating discussion.

References

[1] Kawashima K, Ueda Y, Kosuge K and Kachi S 1974 *J. Crystal Growth* **26** 321
[2] Fisher B and Ron A 1981 *Solid State Commun.* **40** 737
[3] Ueda Y, Kosuge K and Kachi S 1976 *Mater. Res. Bull.* **11** 293
[4] Gustafsson T, Thomas J O, Koksbang R and Farrington G C 1992 *Electrochem. Acta* **37** 1639
[5] Whilhelmi K A, Waltersson K and Khilborg L 1971 *Acta Chem. Scand.* **25** 2675
[6] Dernier P D 1974 *Mater. Res. Bull.* **9** 955
[7] Eguchi R, Yokota T, Kiss T, Ueda Y and Shin S 2002 *Phys. Rev.* B **65** 205124
[8] Itoh M, Yasuoka H, Ueda Y and Kosuge K 1984 *J. Phys. Soc. Japan* **53** 1847

[9] Schulz H J 1991 *Int. J. Mod. Phys.* B **5** 57
[10] Onoda M, Ohta H and Nagasawa H 1991 *Solid State Commun.* **79** 281
[11] Montgomery H C 1971 *J. Appl. Phys.* **42** 2971
[12] Terao M and Ohashi Y 2001 *J. Phys. Soc. Japan* **70** 233
[13] Beni G 1974 *Phys. Rev.* B **10** 2186
[14] Mizokawa T, Fujimori A, Namatame H, Akeyama K and Kosugi N 1994 *Phys. Rev. Lett.* **49** 7193
[15] Cooper J R, Miljak M, Delplanque G, Jérome D, Weger M, Fabre J M and Giral L 1977 *J. de Physique* **38** 1097
[16] Moser J, Cooper J R, Jérome A B, Brown S E and Bechgaard K 2000 *Phys. Rev. Lett.* **84** 2674
[17] Yakovenko V M and Zheleznyak A T 1999 *Synth. Met.* **103** 2202
[18] Usuki T, Kawakami N and Okiji A 1990 *J. Phys. Soc. Japan* **59** 1357
[19] Onoda M and Arai R 2001 *J. Phys.: Condens. Matter* **13** 10399
[20] Onoda M and Hasegawa J 2002 *J. Phys.: Condens. Matter* **14** 5045
[21] Freeman A J and Watson R E 1965 *Magnetism* part A, vol 2, ed G T Rado and H Suhl (New York: Academic)
[22] Onoda M and Kagami T 1999 *J. Phys.: Condens. Matter* **11** 3475, and references therein
[23] Bonner J C and Fisher M E 1964 *Phys. Rev.* **135** A640
[24] For example, Schulz H J 1996 *Phys. Rev. Lett.* **77** 2790
[25] Stafford C A 1993 *Phys. Rev.* B **48** 8430